

Theory of Raman Scattering from Orbital Excitations in Manganese Oxides

S. Okamoto¹, S. Ishihara², and S. Maekawa³

¹The Institute of Physical and Chemical Research (RIKEN), Saitama 351-0198, Japan

²Department of Applied Physics, University of Tokyo, Tokyo 113-8656, Japan

³Institute for Materials Research, Tohoku University, Sendai 980-8577, Japan

(October 30, 2018)

We present a theory of the Raman scattering from the orbital wave excitations in manganese oxides. Two excitation processes of the Raman scattering are proposed. The Raman scattering cross section is formulated by using the pseudospin operator for orbital degree of freedom in a Mn ion. The Raman spectra from the orbital wave excitations are calculated and their implications in the recent experimental results reported in LaMnO₃ are discussed.

PACS numbers: 75.30.Et, 75.30.Vn, 71.10.-w, 78.20.Bh

I. INTRODUCTION

Since the discovery of the colossal magnetoresistance (CMR), much attention has been attracted to manganese oxides with perovskite structure.¹⁻³ A variety of anomalous phenomena including gigantic decrease of the resistivity are observed in the vicinity of the phase transition from the charge and orbital ordered state to the ferromagnetic metallic one in the oxides. One of the key factors to bring about the phenomena is the orbital degree of freedom in a Mn ion.⁴ Due to the strong Hund coupling and crystalline field, two e_g orbitals are degenerate and one of the $3d_{3z^2-r^2}$ and $3d_{x^2-y^2}$ orbitals is occupied by an electron in a Mn³⁺ ion.

Extensive studies of the orbital ordering have been done. It is well known that orbital ordering associated with the Jahn-Teller (JT) type lattice distortion plays an important role to stabilize the layered (A) antiferromagnetic ordering in LaMnO₃, where spins align parallel (antiparallel) in the xy plane (along the z axis).⁵⁻¹² In the doped manganites, a variety of magnetic structures associated with the orbital orderings are reported. On the other hand, the dynamics of the orbital degree of freedom still remains to be clarified. In the orbital ordered state, the collective excitation of the orbital degree of freedom, termed orbital wave, has been theoretically predicted.^{9,13-18} The orbital wave corresponds to the collective electron excitation from occupied orbital to unoccupied one, i. e., the modulation of the shape of electronic cloud. When the orbital wave is excited, various low-energy properties, such as spin wave dispersion¹⁷, phonon dispersion¹⁸, transport¹⁹ and thermodynamic properties, will be largely affected. However, the orbital wave excitations have not been observed because the experimental technique was limited. To clarify the dynamics of the orbital degree of freedom and its effects on the physical properties in manganese oxides, it is indispensable to establish a method to observe the orbital wave.

As a probe to observe the orbital wave, Ishihara *et al.* proposed the resonant inelastic x-ray scattering by which dispersion relation of the orbital wave can be detected.²⁰ One of the other possible method to detect the orbital excitations is the Raman scattering.²¹ Although only the

excitation at $\vec{k} = 0$ and the density of states (DOS) may be detected, the Raman scattering has the following advantages: its energy resolution is of the order of 1 cm⁻¹ which is higher than that of the x-ray scattering and the different modes of the excitations are distinguished by the polarization analyses of the incident and scattered photons. Recently, the Raman scattering experiment in the detwinned single crystal of LaMnO₃ was carried out by Saitoh *et al.*²² They found peak structures around 150 meV. By the detailed analyses of the polarization dependence and the Raman-shift energy of the spectra, the newly found spectra can be attributed to neither the multi-phonon nor the magnon excitations. Therefore, a theory of the Raman scattering from the remaining degree of freedom, i. e., the orbital excitation, is required to be developed.

In this paper, we present a detailed theoretical framework of the Raman scattering from the orbital-wave excitations in orbital ordered manganites. We propose two excitation processes. One of them is analogous to that in the two-magnon Raman scattering in antiferromagnets. However, the intensities of the Raman spectra from one- and two-orbital wave excitations are of the same order of magnitudes in this process, in contrast to the magnon Raman scattering. In another scattering process, photon induces exchange of electrons between Mn e_g and O $2p$ orbitals, and one-orbital wave excitation is brought about. We formulate the scattering cross section by using the pseudospin operator for the orbital degree of freedom in Mn ions. Raman spectra from the orbital wave excitations are calculated as functions of energy in several polarization configurations. It is shown that the recent Raman experiments in LaMnO₃ are well explained by the orbital wave excitations.

In Sec. II, the model Hamiltonian is introduced and dispersion relation of the orbital wave is investigated. In Sec. III and Sec. IV, the excitation processes for the Raman scattering are proposed and the cross section are formulated, respectively. Numerical results are presented in Sec. V, where comparison between theory and experiment is shown. The last section is devoted to the summary and discussion.

II. ORBITAL WAVE

Let us set up the model Hamiltonian describing the electronic state of manganese oxides. We consider the tight-binding Hamiltonian in the cubic lattice consisting of Mn ions. At each site, two e_g orbitals are introduced and t_{2g} electrons are treated as a localized spin ($\vec{S}_{t_{2g}}$) with $S_{t_{2g}} = 3/2$. We introduce three kinds of Coulomb interaction, i. e., the intra- (U) and inter- (U') orbital Coulomb interactions and the exchange interaction (I), between e_g electrons at the same site. The energy splitting between two e_g orbitals due to the JT distortion of a MnO_6 octahedron is represented by $g_{JT}\sqrt{Q_x^2 + Q_z^2}$, where g_{JT} and Q_l are the electron-lattice coupling constant and the normal mode of the lattice distortion, respectively. The Hund coupling (J_H) between e_g and t_{2g} spins and the antiferromagnetic superexchange (SE) interaction (J_{AF}) between nearest neighboring (NN) t_{2g} spins are introduced. Among these energy parameters, the intra-site Coulomb interactions are the largest.²³ Thus, by excluding the doubly occupied states in the e_g orbitals, the following effective Hamiltonian for the low energy electronic state is derived:⁹

$$\tilde{\mathcal{H}} = \mathcal{H}_J + \mathcal{H}_H + \mathcal{H}_{AF} + \mathcal{H}_{JT}. \quad (1)$$

The first term represents the SE interaction between NN e_g electrons given by

$$\begin{aligned} \mathcal{H}_J &= -2J_1 \sum_{\langle ij \rangle} \left(\frac{3}{4} n_i n_j + \vec{S}_i \cdot \vec{S}_j \right) \left(\frac{1}{4} - \tau_i^l \tau_j^l \right) \\ &\quad - 2J_2 \sum_{\langle ij \rangle} \left(\frac{1}{4} n_i n_j - \vec{S}_i \cdot \vec{S}_j \right) \left(\frac{3}{4} + \tau_i^l \tau_j^l + \tau_i^l + \tau_j^l \right), \quad (2) \end{aligned}$$

where J_1 and J_2 are the parameters for the SE interaction. Their definitions are given in Ref. 24. \vec{S}_i is the spin operator of the e_g electron with $S = 1/2$. $\tau_i^l = \cos(\frac{2\pi}{3} m_l) T_{iz} - \sin(\frac{2\pi}{3} m_l) T_{ix}$ with $(m_x, m_y, m_z) = (1, -1, 0)$. l denotes a direction of a bond between site i and site j . \vec{T}_i is the pseudospin operator for the orbital degree of freedom defined by $\vec{T}_i = (1/2) \sum_{\gamma\gamma'\sigma} \tilde{d}_{i\gamma\sigma}^\dagger (\vec{\sigma})_{\gamma\gamma'} \tilde{d}_{i\gamma'\sigma}$ where $\tilde{d}_{i\gamma\sigma}$ is the annihilation operator of the e_g electron at site i with spin σ and orbital γ . This operator excludes the doubly occupied states of electrons. $\langle T_{iz} \rangle = +(-)1/2$ corresponds to the state where the $d_{3z^2-r^2}$ ($d_{x^2-y^2}$) orbital is occupied by an electron. The second and third terms in Eq. (1) are given by

$$\mathcal{H}_H + \mathcal{H}_{AF} = -J_H \sum_i \vec{S}_i \cdot \vec{S}_{t_{2g}i} + J_{AF} \sum_{\langle ij \rangle} \vec{S}_{t_{2g}i} \cdot \vec{S}_{t_{2g}j}. \quad (3)$$

Here, the anisotropy of the SE interaction originating from the tetragonal (D_{4h}) lattice distortion is taken into account as $\sqrt{J_{1(2)}^z/J_{1(2)}^x} = \sqrt{J_{AF}^z/J_{AF}^x} = t_0^z/t_0^x = R$,

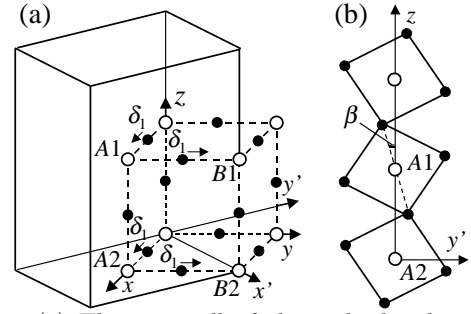


FIG. 1. (a) The unit cell of the orthorhombic structure (straight lines). Open and filled circles represent Mn and O ions, respectively. The unit cell of the cubic perovskite structure is shown by broken lines. Arrows indicate the displacements of O ions in the orthorhombic structures where δ_1 is an amplitude of the displacement. (b) The alternate rotations of MnO_6 octahedra around x' axis. β is an angle of the rotation.

$J_{1(2)}^x = J_{1(2)}^y$ and $J_{AF}^x = J_{AF}^y$. $t_0^{z(x)}$ is the transfer intensity between NN $d_{3z^2-r^2}$ ($d_{x^2-y^2}$) orbitals along the $z(x)$ axis. The last term in Eq. (1) is given by

$$\mathcal{H}_{JT} = -g_{JT} \sum_{i|l=z,x} Q_{il} T_{il}. \quad (4)$$

Q_{il} is defined by $(Q_{iz}, Q_{ix}) = Q(\cos \theta_i^{JT}, \sin \theta_i^{JT})$, where θ_i^{JT} represents the mixing of two normal modes of the lattice distortion. The lattice degree of freedom is assumed to be frozen in this paper, since the electronic process which we are interested in here has much larger energy than the lattice excitations.

We investigate the orbital states at the paramagnetic and A -AF phases by applying the mean field approximation.²⁵ A unit cell which includes four Mn sites is adopted. These Mn sites are termed A_1, A_2, B_1 and B_2 (see Fig. 1). $A(B)$ and $1(2)$ classify the orbital and spin sublattices, respectively. As spin order parameters, we introduce $\langle S_{iz} \rangle$ and $\langle S_{t_{2g}iz} \rangle (= 3\langle S_{iz} \rangle)$, where $\langle \dots \rangle$ represents the thermal average. For the JT distortion of MnO_6 octahedra, C -type ordering with $(\theta_{A1(2)}^{JT}, \theta_{B1(2)}^{JT}) = (2\pi/3, -2\pi/3)$ is adopted by considering the observed lattice distortion in LaMnO_3 . For the orbital degree of freedom, we introduce the rotating frame and adopt the order parameter as $\langle \tilde{T}_{iz} \rangle = \cos \theta_i^t \langle T_{iz} \rangle + \sin \theta_i^t \langle T_{ix} \rangle$. θ_i^t describes the orbital state at site i as $|\theta_i^t\rangle = \cos \frac{\theta_i^t}{2} |3z^2 - r^2\rangle + \sin \frac{\theta_i^t}{2} |x^2 - y^2\rangle$. By minimizing the energy with respect to $\{\theta_i^t\}$, we obtain $(\theta_{A1(2)}^t, \theta_{B1(2)}^t) = (\theta_A, -\theta_A)$ in both the paramagnetic and A -AF phases.

The collective orbital excitations in the orbital ordered state are studied by applying the Holstein-Primakoff transformation to the pseudospin operators. Here, spins are assumed to be frozen. The orbital pseudospin is represented by using the bosonic operator, a_i at site i , as $\tilde{T}_{iz} = 1/2 - a_i^\dagger a_i$ and $\tilde{T}_{ix} = 1/2(a_i^\dagger + a_i)$. In Figs. 2 (a) and (b), the dispersion relation of the orbital waves in the paramagnetic and A -AF states are shown. Paramagnetic

ter values are chosen to be $J_2/J_1 = 0.35$, $R = 1.07$ and $g_{JT}Q/J_1 = 0.7$. J_1 is estimated to be about 50 meV from the dispersion relation of the spin wave, the Néel temperature for A -AF and the orbital ordering temperature. It is shown that the orbital excitation has a gap in both cases. However, we note the origin of these gaps are different as follows: The gaps in paramagnetic and A -AF phases are given by $\sqrt{\frac{\sqrt{3}}{2}g_{JT}Q(\frac{9}{2}J_1 - \frac{1}{2}J_2 + \frac{\sqrt{3}}{2}g_{JT}Q)}$ and $\sqrt{(3J_1 + \frac{\sqrt{3}}{2}g_{JT}Q)(J_1 + J_2 + \frac{\sqrt{3}}{2}g_{JT}Q)}$, respectively, where θ_A is chosen to be $\pi/2$. While the gap in the paramagnetic phase decreases with decreasing $g_{JT}Q$, the gap in the A -AF phase remains finite. This is because the latter originates from the anisotropic magnetic structure.⁹ $\mu = (\pm\pm')$ in Fig. 2 denotes the mode of the orbital wave, where $\pm(\pm')$ represents the relative phase of the Holstein-Primakoff bosons of the four orbital sublattices in the xy plane (along the z axis). Among four modes, $(-+)$ is the highest and its eigenoperator is given by

$$\alpha_k^{(-+)} = \cosh\theta^{(-+)}(a_{A1k} - a_{B1k} + a_{A2k} - a_{B2k}) + \sinh\theta^{(-+)}(a_{A1-k}^\dagger - a_{B1-k}^\dagger + a_{A2-k}^\dagger - a_{B2-k}^\dagger). \quad (5)$$

$\cosh\theta^{(-+)}$ and $\sinh\theta^{(-+)}$ are the coefficients of the Bogoliubov transformation. This eigenoperator includes the following linear combinations of pseudospin operators:

$$\begin{aligned} & \alpha_k^{(-+)} \\ &= \sqrt{\frac{N_m}{N}} \sum_{l(\text{unit cell})} e^{i\vec{k}\cdot\vec{r}_l} \left(\cos\theta_A (\cosh\theta^{(-+)} + \sinh\theta^{(-+)}) \right. \\ & \quad \times (T_{A1(l)x} + e^{ik_y}T_{B1(l)x} + e^{-ik_z}T_{A2(l)x} \\ & \quad \quad \quad \left. + e^{-i(k_y+k_z)}T_{B2(l)x}) \right. \\ & \quad - i(\cosh\theta^{(-+)} - \sinh\theta^{(-+)}) \\ & \quad \times (T_{A1(l)y} - e^{ik_y}T_{B1(l)y} + e^{-ik_z}T_{A2(l)y} \\ & \quad \quad \quad \left. - e^{-i(k_y+k_z)}T_{B2(l)y}) \right). \quad (6) \end{aligned}$$

N_m is the number of sites in the unit cell and the lattice constants are taken to be unity. By using the Group theory, it is shown that the irreducible representations of the modes $(-+)$, $(+-)$, $(--)$ and $(++)$ are identified as A_g , B_{1g} , B_{3g} and B_{2g} in the D_{2h} group, respectively. From the irreducible representations, the allowed-mode symmetries of the orbital waves in several polarization configurations are assigned. Throughout this paper, the polarization configuration is denoted by (ζ, η) where ζ and η ($= x, y, z, x', y'$) represent the polarization of the incident and scattered photons, respectively. Here, x, y and z axes are the directions of the bonds connecting NN Mn sites and x' (y') is defined by $x' = x + y$ ($y' = -x + y$). x', z and $-y'$ axes correspond to a, b and c axes in $Pnma$ structure, respectively. (see Fig. 1) Polarization configurations and the allowed-mode symmetries of the orbital waves are obtained as follows:

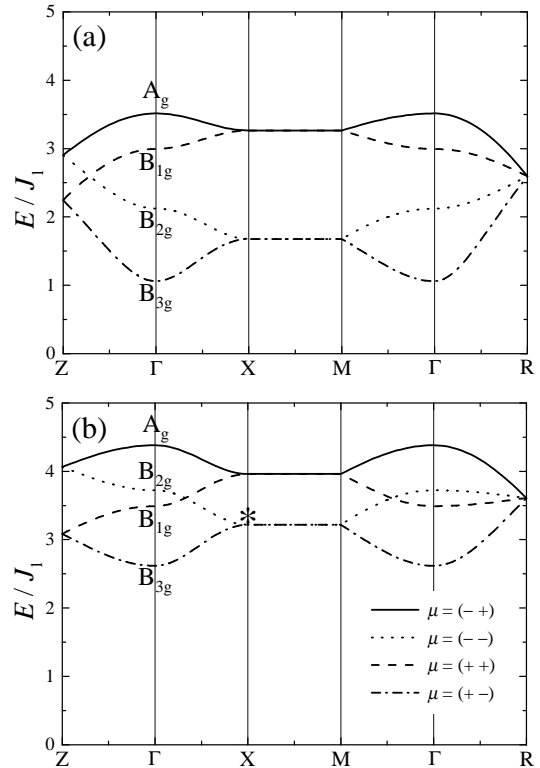


FIG. 2. The dispersion relation of orbital wave in (a) paramagnetic and (b) A -AF phases. The Brillouin zone for the tetragonal lattice is adopted. Parameter values are chosen to be $J_2/J_1 = 0.35$, $R = 1.07$, $g_{JT}Q/J_1 = 0.7$, and $\theta_{A1}^{JT} = 2\pi/3$. Orbital state for the paramagnetic (A -AF) phase is denoted by $(\theta_{A1(2)}, \theta_{B1(2)}) = (\theta_A, -\theta_A)$ with $\theta_A = 0.52\pi$ (0.47π). An asterisk in (b) shows the mode which becomes Raman active when the monoclinic lattice distortion is introduced (See Fig. 7).

$$\begin{aligned} (x, x) & \rightarrow A_g + B_{2g}, \\ (y, y) & \rightarrow A_g + B_{2g}, \\ (z, z) & \rightarrow A_g, \\ (x, y) & \rightarrow A_g, \\ (z, x) & \rightarrow B_{2g} + B_{3g}, \\ (x', x') & \rightarrow A_g, \\ (x', y') & \rightarrow B_{2g}. \end{aligned}$$

III. SCATTERING PROCESSES

In this section, we propose the excitation processes of the orbital wave in the Raman scattering. Here, we consider the Raman scattering experiment carried out by using the visible light. It has been reported that the electronic energy band in the region of $0\sim 3$ eV below the Fermi level in LaMnO_3 consists of Mn e_g and O $2p$ orbitals.²³ Therefore, it is expected that both the Mn e_g and O $2p$ orbitals play important roles in the excitation

processes. Taking into account these facts, the following two excitation processes are considered.

One of the processes is analogous to that in the two-magnon Raman scattering in the antiferromagnet. Mn e_g orbitals are considered and O $2p$ orbitals are integrated out. The schematic picture of this process is presented in Fig. 3 (a). An electron at a Mn e_g orbital is excited to one of NN e_g orbitals through the interaction with an incident photon whose energy, momentum and polarization are denoted as $\hbar\omega_i$, \vec{k}_i and λ_i , respectively. By emitting a photon with $\hbar\omega_f$, \vec{k}_f and λ_f , one of the two electrons at a doubly-occupied Mn site returns to the empty Mn site. When the orbital states at one of the two or both the sites in the final state are different from those in the initial state, one- or two-orbital wave excitations are brought about, respectively. Hereafter, this process is termed the d - d process. It is stressed that the scattering intensities from one- and two-orbital wave excitations are of the same order of magnitudes. This is due to the transfer intensity between the different orbitals at NN Mn sites. This characteristic is highly in contrast to the magnon Raman scattering in the antiferromagnet.^{26–28}

In addition to the d - d process, an orbital excitation is brought about through the exchange of electrons between Mn e_g and O $2p$ orbitals. A schematic picture of this process is presented in Fig. 3 (b). An electron in an O p_σ orbital is excited to the neighboring Mn e_g orbital, where p_σ represents the O $2p$ orbital mixing with the Mn e_g one through the σ bond. There are two electrons in this Mn site and one hole in an O p_σ orbital in the intermediate state. Then, one of the two electrons in this Mn site returns to the O site by emitting a photon. When the occupied orbital in the Mn site in the final state is different from that in the initial state, one-orbital wave excitation is brought about. Hereafter, this process is termed the d - p process. In contrast to either the d - d process or the magnon Raman scattering in the antiferromagnet, one-orbital wave is excited in the d - p process.

IV. RAMAN CROSS SECTION

In this section, we present the formulation for the cross section in the d - d and d - p processes.

A. d - d process

The cross section for the orbital wave excitations is calculated in the system where the e_g electrons and photons are coupled. We adopt the following model Hamiltonian:

$$\mathcal{H}_{d-d} = \mathcal{H}_e^{d-d} + \mathcal{H}_t^{d-d} + \mathcal{H}_{ph} + \mathcal{H}_{e-ph}^{d-d}. \quad (7)$$

The first and the second terms represent the intra-site electron-electron interactions and the electronic transfer between NN sites defined as

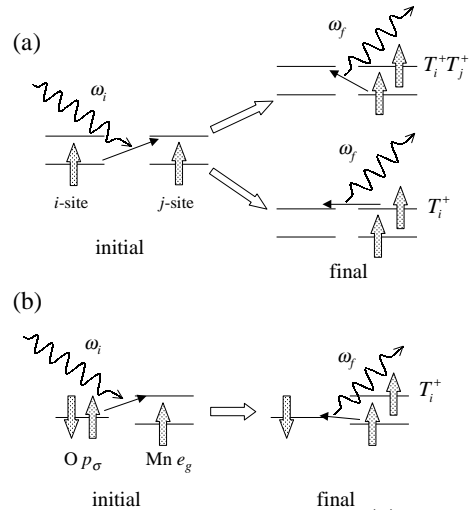


FIG. 3. The excitation processes in the (a) d - d and (b) d - p processes. Wavy lines represent the incident and scattered photons with energy ω_i and ω_f , respectively. i and j in (a) represent NN Mn sites. O p_σ in (b) represents one of the 6 oxygen p_σ orbitals surrounding a Mn ion.

$$\begin{aligned} \mathcal{H}_e^{d-d} &= \mathcal{H}_H + \sum_{i\gamma\sigma} \varepsilon_d d_{i\gamma\sigma}^\dagger d_{i\gamma\sigma} \\ &+ U \sum_{i\gamma} n_{i\gamma\uparrow} n_{i\gamma\downarrow} + U' \sum_{i\gamma\sigma\sigma'} n_{i\gamma\sigma} n_{i-\gamma\sigma'} \\ &+ I \sum_{i\gamma\sigma\sigma'} d_{i\gamma\sigma}^\dagger d_{i-\gamma\sigma}^\dagger d_{i\gamma\sigma'} d_{i-\gamma\sigma'} \end{aligned} \quad (8)$$

and

$$\mathcal{H}_t^{d-d} = \sum_{\substack{\langle ij \rangle \\ \gamma\gamma'\sigma}} \left(t_{ij}^{\gamma\gamma'} d_{i\gamma\sigma}^\dagger d_{j\gamma'\sigma} + \text{H.c.} \right), \quad (9)$$

respectively. $d_{i\gamma\sigma}$ is the annihilation operator of e_g electron at site i with spin σ and orbital γ . Its energy level is given by ε_d . $t_{ij}^{\gamma\gamma'}$ is the transfer intensity between γ orbital at site i and γ' orbital at site j and is obtained by the second-order perturbation with respect to the electron transfer between Mn e_g and O $2p$ orbitals. The explicit form of $t_{ij}^{\gamma\gamma'}$ is given by the Slater-Koster formulas.²⁹ The third term represents the photon system as

$$\mathcal{H}_{ph} = \sum_{\vec{k}\lambda} \hbar\omega_{\vec{k}} \left(b_{\vec{k}\lambda}^\dagger b_{\vec{k}\lambda} + \frac{1}{2} \right), \quad (10)$$

where $b_{\vec{k}\lambda}$ is the annihilation operator of photon with energy $\hbar\omega_{\vec{k}}$, momentum \vec{k} and polarization λ . Finally, the electron-photon interaction is described by the fourth term in Eq. (7) as

$$\mathcal{H}_{e-ph}^{d-d} = -\frac{e}{c} \sum_{\langle ij \rangle \gamma \gamma'} \vec{A}(\vec{r}) \cdot \vec{J}_{ij}^{\gamma\gamma'}. \quad (11)$$

Here, $\vec{A}(\vec{r})$ and $\vec{J}_{ij}^{\gamma\gamma'}$ are the vector potential at $\vec{r} = (\vec{r}_i + \vec{r}_j)/2$ and the current operator, respectively. These are given by

$$\vec{A}(\vec{r}) = \frac{1}{\sqrt{V}} \sum_{\vec{k}\lambda} \sqrt{\frac{2\pi\hbar c^2}{\omega_{\vec{k}}}} \hat{e}_{\lambda} \left(b_{\vec{k}\lambda}^{\dagger} e^{-i\vec{k}\vec{r}} + b_{\vec{k}\lambda} e^{i\vec{k}\vec{r}} \right), \quad (12)$$

and

$$\vec{J}_{ij}^{\gamma\gamma'} = \frac{i}{\hbar} \vec{r}_{ij}^{\dagger} t_{ij}^{\gamma\gamma'} \sum_{\sigma} d_{i\gamma\sigma}^{\dagger} d_{j\gamma'\sigma} + \text{H.c.} \quad (13)$$

\hat{e}_{λ} is the unit vector along the polarization λ and $\vec{r}_{ij} = (\vec{r}_i - \vec{r}_j)$.

Being based on the Hamiltonian \mathcal{H}_{d-d} , the scattering matrix is calculated. The initial and final states of the scattering are described by \mathcal{H} and the intermediate state is described by \mathcal{H}_e^{d-d} . The scattering matrix in the $d-d$ process is obtained as,

$$\begin{aligned} S_{fi}^{d-d} &= \frac{4\pi C i}{V} \delta(E_f - E_i) \sum_{\langle ij \rangle} \left(\hat{e}_{\lambda_f} \cdot \frac{\vec{r}_{ij}}{l_{dd}} \right) \left(\hat{e}_{\lambda_i} \cdot \frac{\vec{r}_{ij}}{l_{dd}} \right) \\ &\times \left(2\tilde{J}_1 \left(\frac{3}{4} n_i n_j + \vec{S}_i \cdot \vec{S}_j \right) \left(\frac{1}{4} - \tau_i^l \tau_j^l \right) \right. \\ &\left. + 2\tilde{J}_2 \left(\frac{1}{4} n_i n_j - \vec{S}_i \cdot \vec{S}_j \right) \left(\frac{3}{4} + \tau_i^l \tau_j^l + \tau_i^l + \tau_j^l \right) \right), \quad (14) \end{aligned}$$

with $C = \pi e^2 / (\hbar^2 \sqrt{\omega_{\vec{k}_i} \omega_{\vec{k}_f}})$. $E_{i(f)}$ represents the energy of the initial (final) state. \tilde{J}_1 and \tilde{J}_2 are defined by $\tilde{J}_1 = l_{dd}^2 t_0^2 / (U' - I + \hbar\omega_{\vec{k}_f}) + l_{dd}^2 t_0^2 / (U' - I - \hbar\omega_{\vec{k}_i})$ and $\tilde{J}_2 = l_{dd}^2 t_0^2 / (U + 2J_H + \hbar\omega_{\vec{k}_f}) + l_{dd}^2 t_0^2 / (U + 2J_H - \hbar\omega_{\vec{k}_i})$, respectively, where l_{dd} is the distance between NN Mn sites. Finally, by rewriting the pseudospin operators in Eq. (14) by using the Holstein-Primakoff bosons, we obtain the cross section in the $d-d$ process as

$$\begin{aligned} I_1^{d-d} &= \frac{\omega_f^2 C^2 N}{\hbar (2\pi c^2)^2} \frac{4}{N_m} \\ &\times \sum_{\mu=1}^{N_m} \left| \sum_{\rho\nu\nu'} (\hat{e}_{\lambda_f} \cdot \vec{\rho}) (\hat{e}_{\lambda_i} \cdot \vec{\rho}) K_{\nu\nu'}^{\rho} (V_{\nu\mu}(0) + W_{\nu\mu}(0)) \right|^2 \\ &\times (n_{\mu 0} \delta(\Delta E + \varepsilon_{\mu 0}) + (1 + n_{\mu 0}) \delta(\Delta E - \varepsilon_{\mu 0})). \quad (15) \end{aligned}$$

$n_{\mu\vec{k}}$ is the number of the boson of mode μ , momentum \vec{k} and energy $\varepsilon_{\mu\vec{k}}$. $V_{\nu\mu}(\vec{k})$ and $W_{\nu\mu}(\vec{k})$ are the coefficients of the Bogoliubov transformation connecting the boson operator for the ν th ion to the μ th eigenmode as

$$a_{\nu\vec{k}} = V_{\nu\mu}(\vec{k}) \alpha_{\mu\vec{k}} + W_{\nu\mu}(\vec{k}) \alpha_{\mu-\vec{k}}^{\dagger}. \quad (16)$$

$K_{\nu\nu'}^{\rho}$ is given by

$$\begin{aligned} K_{\nu\nu'}^{\rho} &= \left(\tilde{J}_1 \left(\frac{3}{4} + S_{\rho} \right) - \tilde{J}_2 \left(\frac{1}{4} - S_{\rho} \right) \right) S_{\nu}^{\rho} C_{\nu'}^{\rho} \\ &\quad - \tilde{J}_2 \left(\frac{1}{4} - S_{\rho} \right) S_{\nu}^{\rho}, \quad (17) \end{aligned}$$

with $S_{\rho} = \langle \vec{S}_i \cdot \vec{S}_{i+\vec{\rho}} \rangle$. S_{ν}^{ρ} and C_{ν}^{ρ} are defined by $S_{\nu}^{\rho} = \sin(\theta_{\nu}^t + \frac{2\pi}{3} m_{\rho})$ and $C_{\nu}^{\rho} = \cos(\theta_{\nu}^t + \frac{2\pi}{3} m_{\rho})$, respectively. $\Delta E (= \hbar\omega_{\vec{k}_i} - \hbar\omega_{\vec{k}_f})$ is the Raman shift energy. The cross section for the two-orbital wave excitation is given by

$$\begin{aligned} I_2^{d-d} &= \frac{\omega_f^2 C^2 N}{\hbar (2\pi c^2)^2} \frac{4}{N_m} \\ &\times \sum_{\vec{k}\mu\mu'} \left| \sum_{\vec{\rho}\nu\nu'} (\hat{e}_{\lambda_f} \cdot \vec{\rho}) (\hat{e}_{\lambda_i} \cdot \vec{\rho}) \left[L_{\nu\nu'}^{\rho} V_{\nu\mu}(\vec{k}) W_{\nu\mu}(-\vec{k}) \right. \right. \\ &\quad \left. \left. + M_{\nu\nu'}^{\rho}(\vec{k}) \delta_{\nu,\nu'+\rho} (V_{\nu\mu}(\vec{k}) + W_{\nu\mu}(\vec{k})) \right. \right. \\ &\quad \left. \left. \times (V_{\nu'\mu'}(-\vec{k}) + W_{\nu'\mu'}(-\vec{k})) \right] \right|^2 \\ &\times (1 + n_{\mu\vec{k}}) (1 + n_{\mu'-\vec{k}}) \delta(\Delta E - \varepsilon_{\mu\vec{k}} - \varepsilon_{\mu'-\vec{k}}), \quad (18) \end{aligned}$$

with

$$\begin{aligned} L_{\nu\nu'}^{\rho} &= \left(\tilde{J}_1 \left(\frac{3}{4} + S_{\rho} \right) - \tilde{J}_2 \left(\frac{1}{4} - S_{\rho} \right) \right) C_{\nu}^{\rho} C_{\nu'}^{\rho} \\ &\quad - 2\tilde{J}_2 \left(\frac{1}{4} - S_{\rho} \right) C_{\nu}^{\rho}, \quad (19) \end{aligned}$$

and

$$\begin{aligned} M_{\nu\nu'}^{\rho}(\vec{k}) &= 2 \left(\tilde{J}_1 \left(\frac{3}{4} + S_{\rho} \right) - \tilde{J}_2 \left(\frac{1}{4} - S_{\rho} \right) \right) \\ &\quad \times S_{\nu}^{\rho} S_{\nu'}^{\rho} \cos k_{\rho}. \quad (20) \end{aligned}$$

In Eq. (18), the anti-Stokes parts are neglected for simplicity. The interaction between two orbital waves in the final state is neglected. This interaction is expected to shift the two-orbital wave Raman spectrum to the lower energy region as the magnon-magnon interaction does in the two-magnon Raman scattering.²⁷

B. $d-p$ process

The cross section from the orbital wave excitation is calculated by using the system where Mn e_g and O p_{σ} orbitals and the electron-photon coupling are taken into account. We start with the following model Hamiltonian:

$$\mathcal{H}_{d-p} = \mathcal{H}_e^{d-p} + \mathcal{H}_t^{d-p} + \mathcal{H}_{ph} + \mathcal{H}_{e-ph}^{d-p}. \quad (21)$$

The first and second terms describe the intra-site electron-electron interactions and electron hopping as $\mathcal{H}_e^{d-p} = \mathcal{H}_e^{d-d} + \frac{1}{2} \sum_{i\delta\sigma} \varepsilon_p p_{i\delta\sigma}^{\dagger} p_{i\delta\sigma}$ and

$$\mathcal{H}_t^{d-p} = \sum_{i\gamma\delta\sigma} \left(t_{\gamma\delta} d_{i\gamma\sigma}^{\dagger} p_{i\delta\sigma} + \text{H.c.} \right), \quad (22)$$

respectively, where ε_p is the energy level of O p_{σ} orbital and $p_{i\delta\sigma}$ is the annihilation operator of the p_{σ} electron at $\vec{r}_i + l_{pd}\vec{\delta}$. l_{pd} is the distance between NN Mn and O sites. $\vec{\delta}$'s are the unit vectors along x, y and z directions.

$t_{\gamma\delta}$ represents the transfer intensity between NN Mn e_g and O p_σ orbitals and is given by

$$t_{\gamma\delta} = t_{pd} \begin{pmatrix} -\frac{1}{2} & -\frac{1}{2} & 1 \\ \frac{\sqrt{3}}{2} & -\frac{\sqrt{3}}{2} & 0 \end{pmatrix}_{\gamma\delta}, \quad (23)$$

for $\delta = x, y, z$ with $t_{\gamma\delta} = -t_{\gamma-\delta}$. t_{pd} is the transfer intensity between Mn $d_{3z^2-r^2}$ orbital at \vec{r}_i and O p_z orbital at $\vec{r}_i + l_{pd}\hat{z}$. The electron-photon interaction is represented by the fourth term,

$$\mathcal{H}_{e-ph}^{d-p} = -\frac{e}{c} \sum_{i\gamma\delta} \vec{A}(\vec{r}_i) \cdot \vec{j}_{i\gamma\delta}. \quad (24)$$

$\vec{j}_{i\gamma\delta}$ is the current operator representing the transition between Mn γ orbital at \vec{r}_i and O p_σ orbital at $\vec{r}_i + l_{pd}\hat{z}$ given by

$$\vec{j}_{i\gamma\delta} = \frac{i}{\hbar} l_{pd} \vec{\delta} t_{\gamma\delta} \sum_{\sigma} d_{i\gamma\sigma}^\dagger p_{i\delta\sigma} + \text{H.c.} \quad (25)$$

The scattering matrix is obtained by the second order perturbation with respect to \mathcal{H}_{e-ph}^{d-p} and is given by

$$S_{fi}^{d-p} = \frac{4\pi C_i}{V} \delta(E_f - E_i) \sum_{i\vec{p}} (\hat{e}_{\lambda_f} \cdot \vec{\rho})(\hat{e}_{\lambda_i} \cdot \vec{\rho}) \tilde{J} \tau_i^p, \quad (26)$$

where $\vec{\rho} = \hat{x}, \hat{y}, \hat{z}$ and

$$\tilde{J} = l_{pd}^2 t_{pd}^2 \left(\frac{\frac{3}{2}}{U' - I - \frac{3}{4}J_H - \Delta + \hbar\omega_{\vec{k}_f}} + \frac{\frac{3}{2}}{U' - I - \frac{3}{4}J_H - \Delta - \hbar\omega_{\vec{k}_i}} - \frac{\frac{1}{2}}{U + \frac{5}{4}J_H - \Delta + \hbar\omega_{\vec{k}_i}} - \frac{\frac{1}{2}}{U + \frac{5}{4}J_H - \Delta - \hbar\omega_{\vec{k}_i}} \right), \quad (27)$$

with $\Delta = \varepsilon_p - \varepsilon_d$. It is worth to mention that S_{fi}^{d-p} includes the linear term of τ_i because the orbital excitation is brought about in a MnO₆ octahedron. Therefore, one-orbital wave excitation contributes to the Raman scattering. Finally, by rewriting the pseudospin operators in Eq. (26) by the Holstein-Primakoff bosons, we obtain the cross section in the $d-p$ process as follows,

$$I^{d-p} = \frac{\omega_f^2 C^2 N}{\hbar(2\pi c^2)^2} \tilde{J}^2 \times \frac{4}{N_m} \sum_{\mu} \left| \sum_{\rho\nu} (\hat{e}_{\lambda_f} \cdot \vec{\rho})(\hat{e}_{\lambda_i} \cdot \vec{\rho}) S_{\nu}^p (V_{\nu\mu 0} + W_{\nu\mu 0}) \right|^2 \times (n_{\mu 0} \delta(\Delta E - \varepsilon_{\mu 0}) + (1 + n_{\mu 0}) \delta(\Delta E + \varepsilon_{\mu 0})). \quad (28)$$

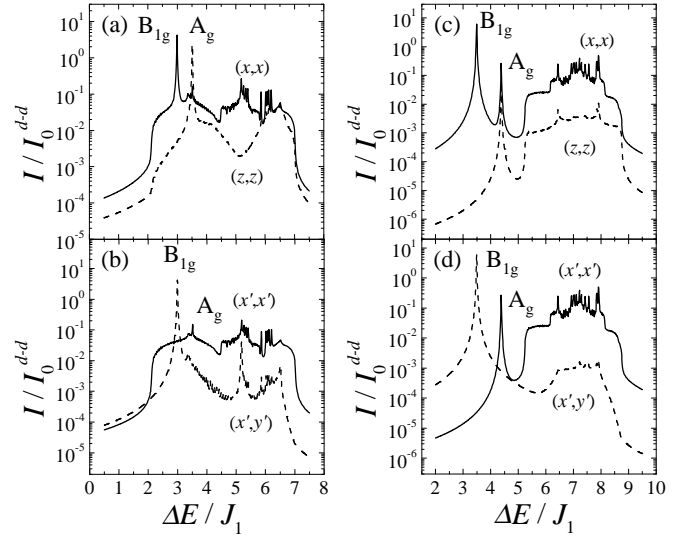


FIG. 4. The Raman scattering spectra from the orbital waves with (a), (b) paramagnetic and (c), (d) A-AF spin structures in the $d-d$ process. I_0^{d-d} is defined by $I_0^{d-d} = \omega_f^2 C^2 N / (\hbar(2\pi)^2) \tilde{J}_1^2$ and is assumed to be independent of ω_i and ω_f , for simplicity. A value of \tilde{J}_2/\tilde{J}_1 is chosen to be 0.35. Other parameter values are the same as those in Fig. 2.

V. NUMERICAL RESULTS

A. $d-d$ process

The Raman scattering spectra in the $d-d$ process are given by the summation of I_1^{d-d} and I_2^{d-d} . Numerical results for the Raman spectra in the paramagnetic and A-AF phases are presented in Fig. 4. Sharp spectra in the region $3.0 < \Delta E/J_1 < 3.6$ ($3.5 < \Delta E/J_1 < 4.5$) and broad ones in the region $2.0 < \Delta E/J_1 < 7.0$ ($5.0 < \Delta E/J_1 < 9.0$) in the paramagnetic (A-AF) phase originate from one- and two-orbital wave excitations, respectively. For the one-orbital wave excitations in the (x, y) and (z, x) polarizations, all modes are Raman inactive as shown in Fig. 4. In these configurations, polarization of the scattered photon is perpendicular to that of the incident photon and both the polarizations are parallel to the bonds between NN Mn sites. Therefore, in these configurations, matrix element S_{fi}^{d-d} in Eq. (14) vanishes and orbital excitations are prohibited. The polarization dependence of the Raman spectra from two-orbital wave excitation are obtained as follows:

$$(x, x), (z, z), (x', x') \text{ and } (x', y') \rightarrow \text{active}, \\ (x, y) \text{ and } (z, x) \rightarrow \text{inactive}.$$

The following relations of the relative intensity are shown: $I(x, x) \sim I(x', x') > I(z, z) \gg I(x', y')$. These relations reflect the type of orbital ordering, that is, the C-type with $\theta_{A1}^t = 0.507\pi$ and 0.481π for paramagnetic and A-AF phases, respectively. Due to this type of orbital ordering, SE interaction between NN e_g electrons

in the xy plane is much stronger than that along the z axis. Therefore, the intensity in the (z, z) polarization is smaller than those in the (x, x) and (x', x') polarizations. Small intensity in the (x', y') configuration is attributed to the interference effect between the orbital waves with the different symmetry. In the spectra from two-orbital wave excitations, several peaks and edges are shown. As the two-magnon Raman spectra reflect the DOS of the magnon, the two-orbital wave Raman spectra reflects the DOS of the orbital waves; position of the each peak corresponds to the van Hove singularity of DOS of the orbital waves. However, the spectra are not the DOS of the orbital waves itself because of the k dependence of the matrix elements $M_{\nu\nu'}^p$. The d - d process may be useful to examine DOS of the orbital waves as well as its excitation with $\vec{k} = 0$.

B. d - p process

In Fig. 5, numerical results of the Raman spectra for the d - p process in the paramagnetic and A -AF phases are shown. We find that the relative intensity of the two spectra from the A_g and B_{1g} modes in the (x, x) configuration in the d - p process is different from that in the d - d process, i. e., the spectrum of the A_g mode becomes larger than that of the B_{1g} mode in the d - p process. As shown in Eq. (6), in the A_g mode, the orbital excitation at each site occurs in-phase. Therefore, interference effect in the in-phase A_g mode increases its intensity in the d - p process. On the other hand, in the d - d process, orbital excitation is dominated by the process where the two electrons in the NN Mn sites are exchanged with each other. Because a minus sign in the scattering matrix arises from the exchange of electrons, interference effects do not occur. This reflects the AF-type orbital ordering in the ground state.

C. Effect of the lattice distortion

In the previous subsections, the Raman scattering spectra have been calculated in the orthorhombic crystal structure. However, it is reported that the lattice structure of LaMnO_3 is monoclinic when the oxygen partial pressure during synthesis is reduced.³⁰ Actually, a sample used in the recent Raman scattering experiments shows the monoclinic structure.³¹ Therefore, we examine the effect of the monoclinic distortion on the Raman spectra in order to compare the present theory with the experiments.

We adopt a model of the crystal structure which is schematically shown in Fig. 6. Displacements of the O ions indicated by arrows are taken into account up to the order of $O(\delta_i/l_{pd})$ as follows. The transfer intensity between NN Mn e_g orbitals in the xy plane is given by $t_0^{xy}(\delta) = t_0(0)(1 + \delta/l_{pd})^{3.5}(1 - \delta/l_{pd})^{3.5}$. Therefore,

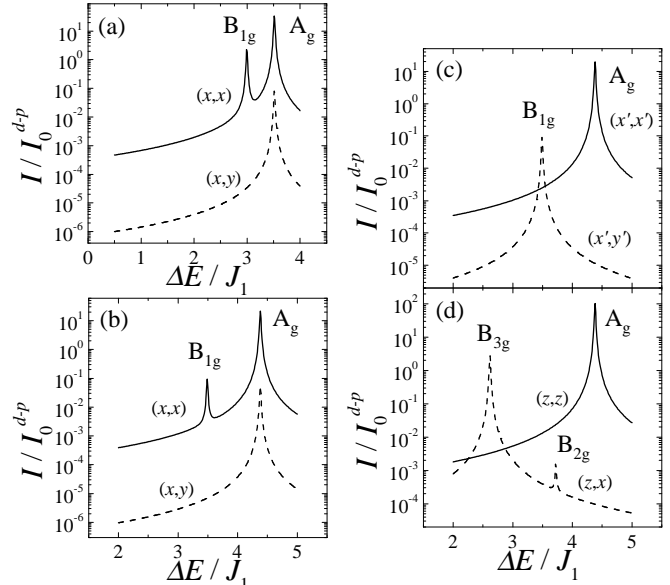


FIG. 5. The Raman scattering spectra from the orbital waves in (a) the paramagnetic and (b)-(d) A -AF phases in the d - p process. I_0^{d-p} is defined by $I_0^{d-p} = \omega_f^2 C^2 N / (\hbar(2\pi)^2) \tilde{J}^2$ and is assumed to be independent of $\omega_{i,f}$, for simplicity. The displacement of the O ions and the rotation of MnO_6 octahedra are set to be $\delta_1/l_{pd} = 0.04$ and $\beta = \frac{\pi}{18}$. Other parameter values are the same as those in Fig. 2.

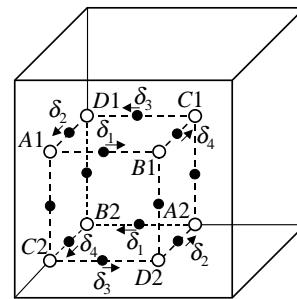


FIG. 6. The unit cell of the monoclinic structures (straight lines). Open and filled circles represent Mn and O ions, respectively. The unit cell of the cubic perovskite structure is shown by broken lines. The arrows indicate the displacement of O ions in the monoclinic structure where δ_{1-4} is the amplitude of the displacement. The alternate rotations of MnO_6 octahedra around x' axis are shown in Fig. 1 (b).

t_0^{xy} does not change within the order of $O(\delta_i/l_{pd})$. $J_{1,2}^{xy}$ does not change, either, because $J_{1,2}^{xy}$ are proportional to $(t_0^{xy})^2$. The transfer intensity between NN Mn e_g and O $2p$ orbitals changes as $t_{pd}(\delta) = t_{pd}(0)(1 \pm 3.5\delta/l_{pd})$. From these facts, the dispersion relation of the orbital wave and the Raman spectra in the d - d process are insensitive to the oxygen displacement but the spectra in the d - p process are sensitive. Therefore, in the following, we concentrate on the d - p process. The dispersion relation of the orbital waves is calculated in the unit cell which includes 8 Mn sites.

In Fig. 7, the numerical results for the d - p process in the monoclinic lattice are shown. Here, A -AF structure is adopted. In addition to the spectra which appear in the orthorhombic lattice, new spectra marked by M are found. Spectral intensity of the peaks M are small compared with others. This is because the distortion from the orthorhombic structure is small. The new peaks at $3.6 J_1$ and $4.4 J_1$ originate from the fact that the mirror symmetry perpendicular to the z axis is absent in the monoclinic structure $P2_1/c$.³⁰ Most strikingly, there appears a new peak at $3.1 J_1$. The peak position corresponds to the energy of the orbital wave at the X point marked by an asterisk in the Fig. 2 (b). This mode becomes zone center mode in the Brillouin zone for the monoclinic lattice and becomes Raman-active.

Now, let us compare our theoretical results with the experimental ones. Recently, Saitoh *et al.* have reported the experimental results of the Raman scattering in a detwinned single crystal of LaMnO_3 .²² In addition to the phonon Raman spectra below 100 meV,^{32,33} sharp spectra in several polarization configurations at 120~170 meV are observed as shown in the insets of Fig. 7. The Raman spectra observed in such a high energy region are usually attributed to the multi-phonon excitations in transition-metal oxides.³⁴ However, by comparing the polarization and the temperature dependence of the new spectra with those of the phonon ones, the possibility of the multi-phonon excitation is ruled out. Two-magnon excitations are also ruled out because spins are ferromagnetically aligned in the xy plane below T_N . As a result, orbital wave is considered as a candidate for the remaining excitation. The crystal structure of the sample in these experiments is monoclinic because of the oxygen partial pressure during synthesis.³⁰ In this experiments, the 514.5 nm line (2.4 eV) of an Ar^+ laser was used. This energy 2.4 eV corresponds to the charge-transfer excitation from O $2p$ to Mn e_g orbitals.³⁵ Therefore, these experimental results are compared with our theoretical ones in the d - p process in the monoclinic lattice. As shown in Fig. 7, the characteristic features of polarization dependence and relative intensity of the experimental Raman spectra in the region of 120~170 meV are well reproduced by our theoretical ones. Thus, the Raman spectra observed in the region of 120~170 meV in LaMnO_3 are attributed to the orbital wave excitations.

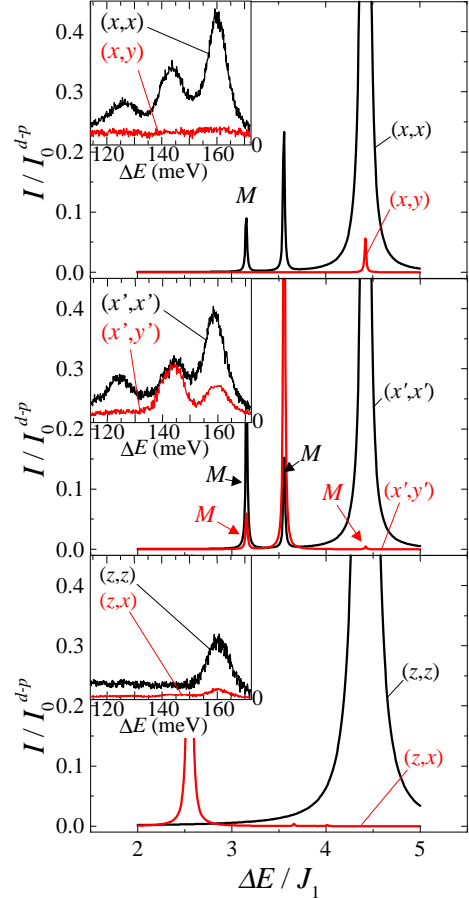


FIG. 7. The Raman scattering spectra from the orbital wave in the A -AF phase. The d - p process in the monoclinic lattice distortion is assumed. The displacement of the O ions and the rotation of MnO_6 octahedra are chosen to be $\delta_1/l_{pd} = 0.03$, $\delta_2/l_{pd} = 0.11$, $\delta_3/l_{pd} = 0.07$, $\delta_4/l_{pd} = 0.15$ and $\beta = \frac{\pi}{18}$. The anisotropy in the transfer intensity is chosen to be $R = 1.15$. Other parameter values are the same as those in Fig. 2. Orbital state is given by $(\theta_{A1(2)}, \theta_{B1(2)}, \theta_{C1(2)}, \theta_{D1(2)}) = (\theta_A, -\theta_A, \theta_A, -\theta_A)$ with $\theta_A = 0.47\pi$. Insets show the experimental Raman spectra in LaMnO_3 at 9 K in Ref. 21. Vertical axes of the experimental data are arbitrary.

VI. SUMMARY AND DISCUSSION

In this study, we have theoretically investigated the Raman scattering as a probe to detect the orbital wave excitations in orbital ordered manganites. Two excitation processes were proposed for the Raman scattering, i.e., the $d-d$ and $d-p$ processes. The $d-d$ process is analogous to the two-magnon Raman scattering process in the antiferromagnet. However, scattering intensity from one- and two-orbital wave excitations are of the same order of magnitude unlike the two-magnon Raman scattering. This is due to the transfer intensity between the NN different orbitals. In the $d-p$ process, photon induces an exchange of electrons between Mn e_g and O $2p$ orbitals, and one-orbital excitations are brought about. Because LaMnO_3 is a charge-transfer type insulator where the optical gap is about 1 eV, the $d-p$ process is expected to dominate the Raman scattering when the visible light is used. It was shown that the theoretical results of the Raman spectra from the one-orbital wave excitations well explain the experimental spectra observed in the region of 120~170 meV in LaMnO_3 .

As mentioned in Sec. II, the orbital wave in the A -AF phase has a gap originating from the anisotropic spin structure. Therefore, we expect that the gap is suppressed by applying a magnetic field. This change will be reflected on the peak positions of the orbital-wave Raman spectra and will be experimentally detected. Similarly, the gap-less orbital wave excitation may be observed in the ferromagnetic-insulating manganites such as $\text{La}_{0.88}\text{Sr}_{0.12}\text{MnO}_3$ where the orbital ordering is experimentally confirmed.³⁶ In Sec. V, we compared the theoretical results for the $d-p$ process with the recent experiments in Ref. 22. This is because the $d-p$ process is dominant in the adopted energy of the incident photon. By changing the incident photon energy, the $d-d$ process may contribute to the scattering. It is expected that the spectral intensities for the $d-d$ process are enhanced with increasing the energy of the incident photon and resonating with the excitation energy from the occupied lower Hubbard band to the unoccupied upper Hubbard one. When the Raman experiment using such a high-energy photon is carried out, we expect that the comparison between the present theoretical results for the $d-d$ process and experiments will provide much information about the orbital wave. It is expected that the Raman spectra from the two-orbital wave excitation will be observed around 200~350 meV in LaMnO_3 .

ACKNOWLEDGMENTS

The authors would like to thank Y. Tokura, E. Saitoh, T. Takahashi, K. Tobe, K. Yamamoto and T. Kimura for their valuable discussions and providing us experimental data before publication. Fruitful discussions with P. Prelovšek, G. Khaliullin and K. Tsuda are also ac-

knowledged. This work was supported by Grant-in-Aid for Scientific Research Priority Area from the Ministry of Education, Science, Sports, Culture and Technology of Japan, CREST Japan and Science and Technology Special Coordination Fund for Promoting Science and Technology. Part of the numerical calculation was performed in the supercomputing facilities in IMR, Tohoku University. One of the authors (S. M.) acknowledges support of the Humboldt Foundation.

-
- ¹ K. Chahara, T. Ohono, M. Kasai, Y. Kanke, and Y. Kozono, *Appl. Phys. Lett.* **62**, 780 (1993).
 - ² R. von Helmolt, J. Wecker, B. Holzapfel, L. Schultz, and K. Samwer, *Phys. Rev. Lett.* **71**, 2331 (1993).
 - ³ Y. Tokura, A. Urushibara, Y. Moritomo, T. Arima, A. Asamitsu, G. Kido, and N. Furukawa, *J. Phys. Soc. Jpn.* **63**, 3931 (1994).
 - ⁴ Y. Tokura and N. Nagaosa, *Science* **288**, 462 (2000).
 - ⁵ J. B. Goodenough, *Phys. Rev.* **100**, 564 (1955), and in *Progress in Solid State Chemistry*, edited by H. Reiss (Pergamon, London, 1971), Vol. 5.
 - ⁶ J. Kanamori, *J. Phys. Chem. Sol.* **10**, 87 (1959).
 - ⁷ G. Matsumoto, *J. Phys. Soc. Jpn.* **29**, 606 (1970).
 - ⁸ K. Hirota, N. Kaneko, A. Nishizawa, and Y. Endoh, *J. Phys. Soc. Jpn.* **65**, 3736 (1996); F. Moussa, M. Hennion, J. Rodriguez-Carvajal, H. Moudden, L. Pinsard, and A. Revcolevschi, *Phys. Rev. B* **54**, 15149 (1996).
 - ⁹ S. Ishihara, J. Inoue, and S. Maekawa, *Physica C* **263**, 130 (1996), and *Phys. Rev. B* **55**, 8280 (1997).
 - ¹⁰ Y. Murakami, J. P. Hill, D. Gibbs, M. Blume, I. Koyama, M. Tanaka, H. Kawata, T. Arima, Y. Tokura, K. Hirota, and Y. Endoh, *Phys. Rev. Lett.* **81**, 582 (1998).
 - ¹¹ J. Rodriguez-Carvajal, M. Hennion, F. Moussa, A. H. Moudden, L. Pinsard, and A. Revcolevschi *Phys. Rev. B* **57**, R3189 (1998).
 - ¹² R. Maezono, S. Ishihara, and N. Nagaosa, *Phys. Rev. B* **57**, R13993 (1998).
 - ¹³ M. Cyrot and C. Lyon-Caen, *J. Phys. (Paris)* **36**, 253 (1975).
 - ¹⁴ G. Khaliullin and V. Oudovenko, *Phys. Rev. B* **56**, R14243 (1997).
 - ¹⁵ L. F. Feiner, A. M. Oleś, and J. Zaanen, *J. Phys.: Condens. Matter* **10**, L555 (1998).
 - ¹⁶ G. Khaliullin and R. Kilian, *J. Phys.: Condens. Matter* **11**, 9757 (1999).
 - ¹⁷ J. van den Brink, W. Stekelenburg, D. I. Khomskii, G. A. Sawatzky, and K. I. Kugel, *Phys. Rev. B* **58**, 10276 (1998).
 - ¹⁸ V. Perebeinos and P. B. Allen, *Phys. Status Solidi B* **215**, 607 (1999).
 - ¹⁹ S. Ishihara, M. Yamanaka, and N. Nagaosa, *Phys. Rev. B* **56**, 686 (1997).
 - ²⁰ S. Ishihara and S. Maekawa, *Phys. Rev. B* **62**, 2338 (2000).
 - ²¹ J. Inoue, S. Okamoto, S. Ishihara, W. Koshibae, Y. Kawamura, and S. Maekawa, *Physica B* **237-238**, 51 (1997).

- ²² E. Saitoh, S. Okamoto, K. Takahashi, K. Tobe, K. Yamamoto, T. Kimura, S. Ishihara, S. Maekawa, and Y. Tokura, *Nature* **410**, 180 (2001).
- ²³ T. Saitoh, A. E. Bocquet, T. Mizokawa, H. Namatame, A. Fujimori, M. Abbate, Y. Takeda, and M. Takano, *Phys. Rev. B* **51**, 13942 (1995).
- ²⁴ J_1 and J_2 are defined by $J_1 = t_0^2/(U' - I)$ and $J_2 = t_0^2/(U' + I + 2J_H)$, respectively, where a relation $U = U' + I$ is assumed. t_0 is the transfer intensity between NN $d_{3z^2-r^2}$ orbitals along the z axis. Energy splitting due to the JT effect is neglected in the denominators because the splitting is much smaller than the Coulomb interactions.
- ²⁵ S. Okamoto, S. Ishihara, and S. Maekawa, *Phys. Rev. B* **61**, 451 (2000), *ibid.* 14647 (2000).
- ²⁶ P. A. Fleury and R. Loudon, *Phys. Rev.* **166**, 514 (1968).
- ²⁷ R. J. Elliott, M. F. Thorpe, G. F. Imbusch, R. Loudon, and J. B. Parkinson, *Phys. Rev. Lett.* **21**, 147 (1968).
- ²⁸ B. S. Shastry and B. I. Shraiman, *Phys. Rev. Lett.* **65**, 1068 (1990).
- ²⁹ J. C. Slater, and G. F. Koster, *Phys. Rev.* **94**, 1498 (1954); W. A. Harrison, in *Electronic Structure and the Properties of Solids, The Physics of the Chemical Bond*, W.H. Freeman and Company, San Francisco (1980).
- ³⁰ J. F. Mitchell, D. N. Argyriou, C. D. Potter, D. G. Hinks, J. D. Jorgensen, and S. D. Bader, *Phys. Rev. B* **54**, 6172 (1996).
- ³¹ K. Tsuda, Y. Ogata, M. Tanaka, E. Saitoh, T. Kimura, and Y. Tokura, (unpublished); Meeting Abstracts of the Physical Society of Japan, Volume 56, Issue 1, Part 3, 454 (2001).
- ³² K. Yamamoto, Master thesis, University of Tokyo, 1996.
- ³³ M. N. Iliev, M. V. Abrashev, H.-G. Lee, V. N. Popov, Y. Y. Sun, C. Thomsen, R. L. Meng, and C. W. Chu, *Phys. Rev. B* **57**, 2872 (1998).
- ³⁴ D. B. Romero, Y. Moritomo, J. F. Mitchell, and H. D. Drew, *Phys. Rev. B* **63**, 132404 (2001).
- ³⁵ T. Arima, Y. Tokura, and J. B. Torrance, *Phys. Rev. B* **48**, 17006 (1993); T. Arima and Y. Tokura, *J. Phys. Soc. Jpn.* **64**, 2488 (1995).
- ³⁶ Y. Endoh, K. Hirota, S. Ishihara, S. Okamoto, Y. Murakami, A. Nishizawa, T. Fukuda, H. Kimura, H. Nojiri, K. Kaneko, and S. Maekawa, *Phys. Rev. Lett.* **82**, 4328 (1999).